machines

MDPI

*Article*

# Effect of 3D Printing Orientation on the Accuracy and Surface Roughness of Polycarbonate Samples

**Paweł Turek *, Anna Bazan and Marcin Bulicz**

Department of Manufacturing Techniques and Automation, Rzeszów University of Technology, 35-959 Rzeszów, Poland; abazan@prz.edu.pl (A.B.); mbulicz1007@gmail.com (M.B.)
* Correspondence: pturek@prz.edu.pl

**Abstract:** The study evaluates models produced using fused deposition modeling (FDM) technology in five orientations, fabricated from polycarbonate (PC) material with a FORTUS 360mc printer. The models included simple shapes (planes and cylinders) and complex free-form surfaces. Accuracy was assessed using a GOM Scan 1 scanner and GOM Inspect 2019 software, focusing on 3D deviations and dimensional and geometric deviations (form, position, and orientation, which have not yet been analyzed in similar studies and may limit the usage of the printed elements). Surface roughness was analyzed using a MarSurf XR profilometer, measuring *Ra* and *Rz* parameters. All models were characterized by a predominance of negative 3D deviations. The analysis of variance showed no effect of model orientation on the values of linear dimensional deviations and geometric deviations. The largest deviations were negative and associated with the size of the models. The average value of the absolute deviation of linear dimensions associated with the size of the model was 0.30 mm. The average value of the absolute deviation of other linear dimensions was 0.07 mm. The average value of orientation and position deviations for each model varied in the range of 0.15–0.20 mm, and for form deviation 0.16–0.20 mm. One of the models had a higher surface roughness (*Ra* = 17.2 µm, *Rz* = 71.3 µm) than the other four models (*Ra* in the range of 12.7–13.8 µm, *Rz* in the range of 57.2–61.2 µm). During the research, three distinct surface types were identified on the models. The research indicated the validity of taking surface type into account when analyzing its microgeometry.

**Keywords:** additive manufacturing; fused deposition modelling; geometrical accuracy; surface roughness; model orientation

check for updates

Academic Editor: Sheng Li

Received: 27 November 2024
Revised: 20 December 2024
Accepted: 26 December 2024
Published: 27 December 2024

**Citation:** Turek, P.; Bazan, A.; Bulicz, M. Effect of 3D Printing Orientation on the Accuracy and Surface Roughness of Polycarbonate Samples. *Machines* **2025**, *13*, 9. https://doi.org/10.3390/machines13010009

**Copyright:** © 2024 by the authors. Licensee MDPI, Basel, Switzerland. This article is an open access article distributed under the terms and conditions of the Creative Commons Attribution (CC BY) license (https://creativecommons.org/licenses/by/4.0/).

## 1. Introduction

Additive manufacturing (AM) techniques are among the fastest-growing technologies, capable of producing even the most geometrically complex models [1,2]. Manufacturing a model using these techniques involves applying material in layers until the complete model is formed [3]. There are a variety of additive manufacturing methods available on the market. In collaboration, the International Organization for Standardization (ISO) and the American Society for Testing and Materials (ASTM) have developed ISO/ASTM 52900 [4] and ISO/ASTM 52910 [5] to standardize the additive techniques currently in use. The main differences among the various additive methods lie in how successive layers are cured and the type of material used [6]. Due to the wide availability of materials and their relatively low cost compared with other 3D printing options, material extrusion (MEX) has become the most common method used in additive manufacturing. Models created using this method are utilized in several industries, including aerospace [7,8], automotive [9,10], and medical sectors [11–13].

By selecting appropriate technological parameters during the manufacturing of a model, the geometry can be adjusted to meet specific technical requirements. Evaluating the resulting surface texture is crucial for objects produced using additive manufacturing methods [14–17]. Each 3D printer operates with unique characteristics and specific requirements related to its operating conditions. In the case of the material extrusion (MEX) method, particular attention should be given to factors such as the temperature in the 3D printer's workspace [18], the temperature of the nozzle, and the work platform [18]. Additional factors that can affect accuracy include:

- Layer thickness [19,20];
- Manufacturing speed [21];
- The orientation of the model within the 3D printer [22,23];
- The degree of model filling [24];
- The types of model and support materials used [25,26].

These elements play a significant role in achieving high-quality manufactured models. However, the most significant factor affecting the accuracy of geometry in MEX technology is the layer thickness and the model's orientation within the 3D printer. Freeform surfaces or those inclined at non-90° angles to the layering direction are particularly sensitive to changes in model orientation [27–29]. Basic information about the model's orientation in the 3D printer is provided through ISO 17295 [30]; however, it lacks detailed information regarding its impact on manufacturing accuracy. Additionally, the structure that supports the model during the manufacturing process also influences the accuracy of the final geometry. This often necessitates post-processing treatment to remove the support material through mechanical or chemical methods [31,32]. Consequently, after removing the support material, the model's surface may differ from the designer's initial specifications concerning dimensional and geometrical accuracy and surface roughness.

Because functional models are often produced using additive technology, quality requirements regarding dimensional and geometrical accuracy are imposed on them. The most common standards used in the design process are ISO 8015 [33], ISO 1101 [34], ISO 286-2 [35], ISO 22081 [36], and ASME Y14.5 [37], among others. Regarding surface roughness, ISO 21920 [38–40] is mainly used to describe the design object correctly. However, the standards primarily presented refer to the accuracy obtained using traditional (e.g., subtractive) methods of manufacturing the finished product. The standards that relate directly to additive methods still require development, as this can allow the following:

- Achieving the expected geometric accuracy of the objects, which will allow, among other things, the appropriate adjustment of parts in the assembly process;
- Control of the production process by, among other things, selecting the optimum 3D printing parameters to achieve the expected assumptions related to the dimensional and shape accuracy and surface roughness;
- Avoiding the generation of a large amount of waste samples that do not meet the design assumptions;
- Avoiding time-consuming and often expensive post-processing and surface finishing methods to achieve the required specifications;
- Improvement in energy efficiency, achieved by adapting the technical parameters of the 3D printers to the designer's recommendations;
- Optimization of 3D printing time, which may involve a reduction in the cost of manufacturing the model;
- Increasing the competitiveness of 3D printing methods in manufacturing functional components.

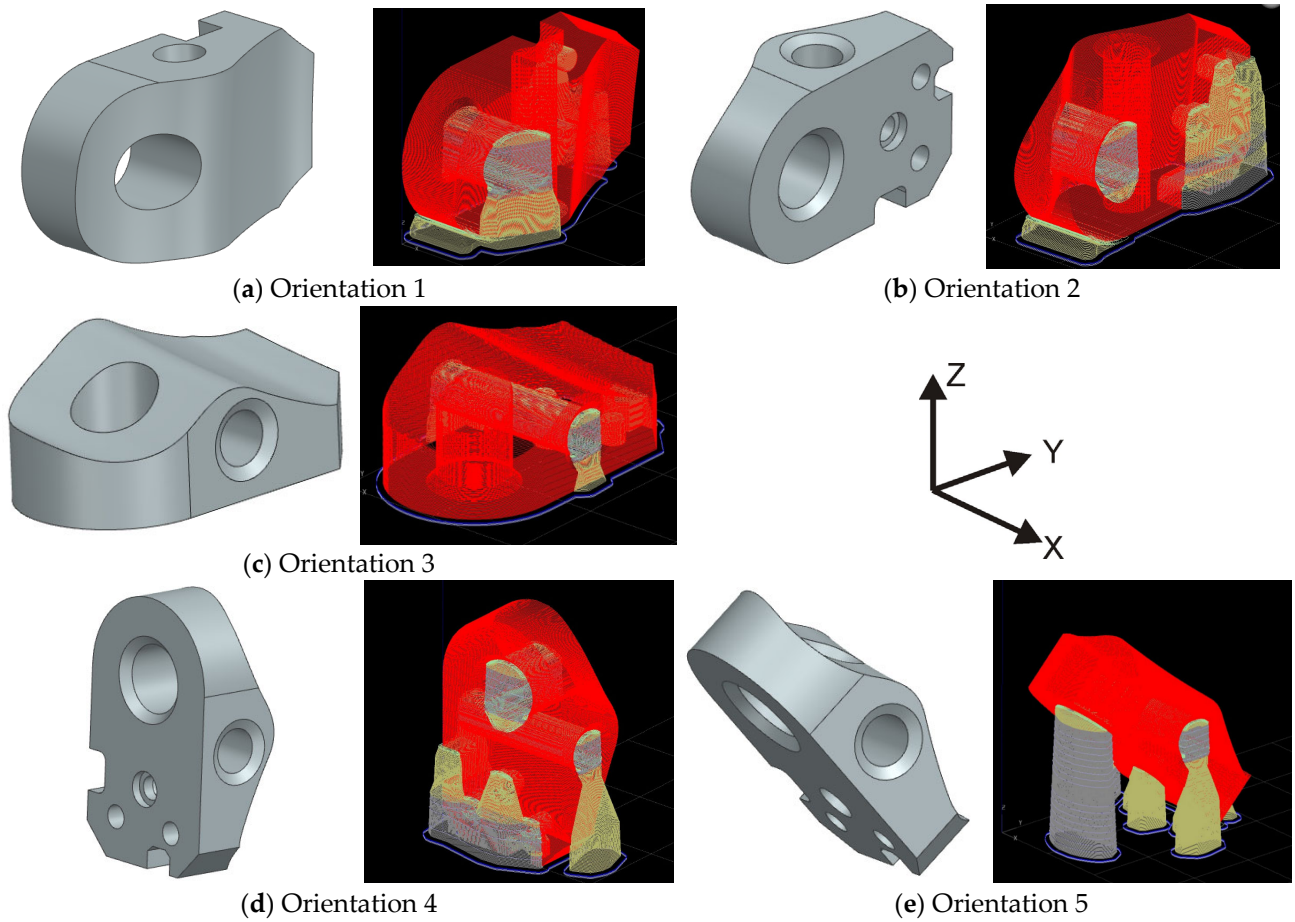
Additional standards are needed to evaluate geometric accuracy and surface roughness in additive manufacturing. The lack of design guidelines for dimensional and geometrical accuracy and surface roughness in additive manufacturing presents challenges for commercializing products in industries like aerospace and automotive. This article evaluates the effect of changing the model's orientation in the 3D printer space on the dimensional and geometrical accuracy and surface roughness of a model made of PC-10 material using the fused deposition modelling (FDM) method. Five characteristic orientations of the model in the 3D printer space were used in the manufacturing process. The geometry was measured using a GOM Scan 1 (Carl Zeiss AG, Jena, Germany) optical system, and the surface roughness was measured using a MarSurf XR 20 (Mahr GmbH, Göttingen, Germany). The results of the measurements were then processed based on the model orientation that generated the linear, form deviations, and surface roughness parameters.

The novelty of this study lies in its comprehensive assessment of geometrical accuracy for 3D printed models made from PC material using FDM technology. Similar previous studies have primarily focused on evaluating 3D deviations and surface roughness. In contrast, this research incorporates the analysis of geometrical deviations, including form, position, and orientation deviations. Additionally, it introduces the consideration of surface type in roughness analysis, distinguishing between surfaces formed as the final material layer, those in contact with support material, or those that consist of successive layers of deposited filament.

## 2. Materials and Methods

A 3D CAD research model was created using Siemens NX 2306 software. This model featured various surface types, including planar, cylindrical, conical, and freeform surfaces (Figure 1). Before starting the 3D printing process, the 3D-STL model was uploaded into Insight software. The software slices the model into layers and generates the necessary supports. While slicing the model, the complete model-filling option was applied. When choosing the parameter for visible surfaces, the enhanced setting was selected to ensure the best possible representation of the manufactured surface. The enhanced option narrows and tightly packs the toolpaths for exposed surfaces. The breakaway option was included to facilitate easier removal of supports. T12 printheads were used to print the PC-10 material with a layer thickness of 0.178 mm. This is the highest resolution achievable along the *Z*-axis on the Fortus 360 mc 3D printer (Stratasys, Rechovot, Israel) for this specific material. The models were manufactured in five different orientations within the 3D printer space, as depicted in Figure 1.

The PC-10 material reached its ductile temperature of 365 °C during printing. The 3D printer system maintained a constant thermal condition of 145 °C for the PC-10 material. The models were printed in a closed environment, and the PC-10 material was mechanically removed. Once the models were produced, the next step was to digitize their geometry. For this purpose, a GOM Scan 1 scanner was used. This scanner consists of a stand on which the scanning head is mounted, a rotary table, and a computer workstation (Figure 2a). The GOM Scan 1 projects structured light stripes onto the object. Cameras mounted on the device capture the deformation of these stripes as they interact with the measuring object (Figure 2b). The resulting measurement data creates a three-dimensional point cloud, with coordinates expressed in the scanner's global coordinate system. These data are saved in a stereolithography (STL) file. Before measuring the geometry of the models, a calibration process was conducted according to VDI/VDE 2634 standards. The models were measured using the parameters outlined in Table 1.

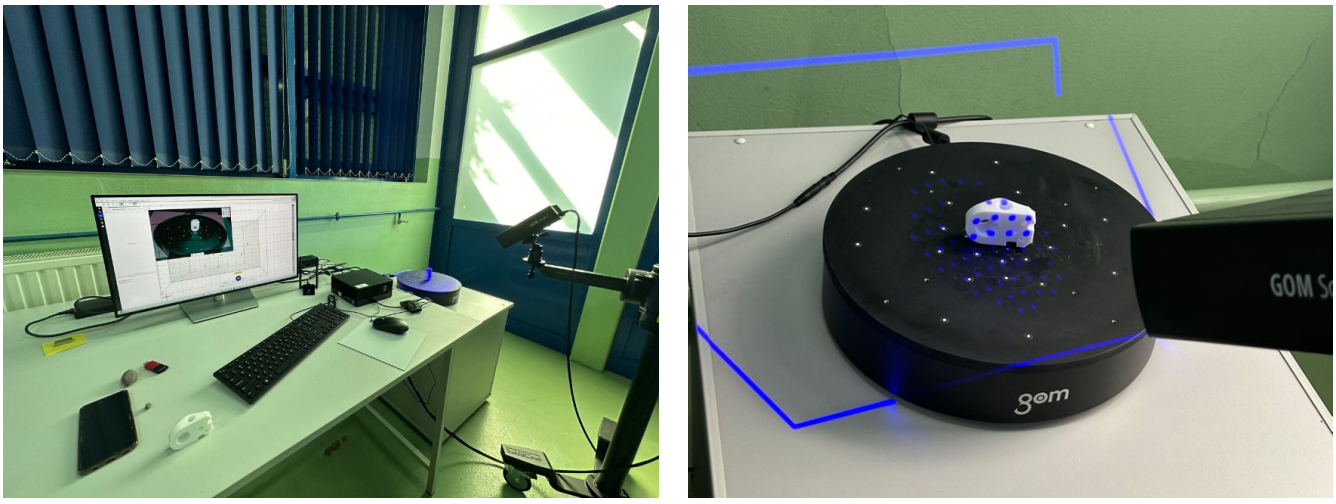



(**a**) Orientation 1 (**b**) Orientation 2

(**c**) Orientation 3

(**d**) Orientation 4 (**e**) Orientation 5

**Figure 1.** Orientation of models in printer space in rendered view (left) and with layer division and support material (right): (**a**) Orientation 1; (**b**) Orientation 2; (**c**) Orientation 3; (**d**) Orientation 4; (**e**) Orientation 5.



(**a**) (**b**)

**Figure 2.** Measurement of the geometry of the manufactured test models: (**a**) Measuring station; (**b**) measuring table with a test model.

The measurement resolution was required to be no more than 10% of the model's tolerance field. Based on published data, the maximum deviation values for models manufactured with a Fortus 360-mc 3D printer using PC-10 material typically fall within ± 0.3 mm [25]. Therefore, the accuracy tolerance for these models was set at 0.6 mm. Given this context, an acceptable measurement resolution of 0.06 mm was established. To address the reflectivity of

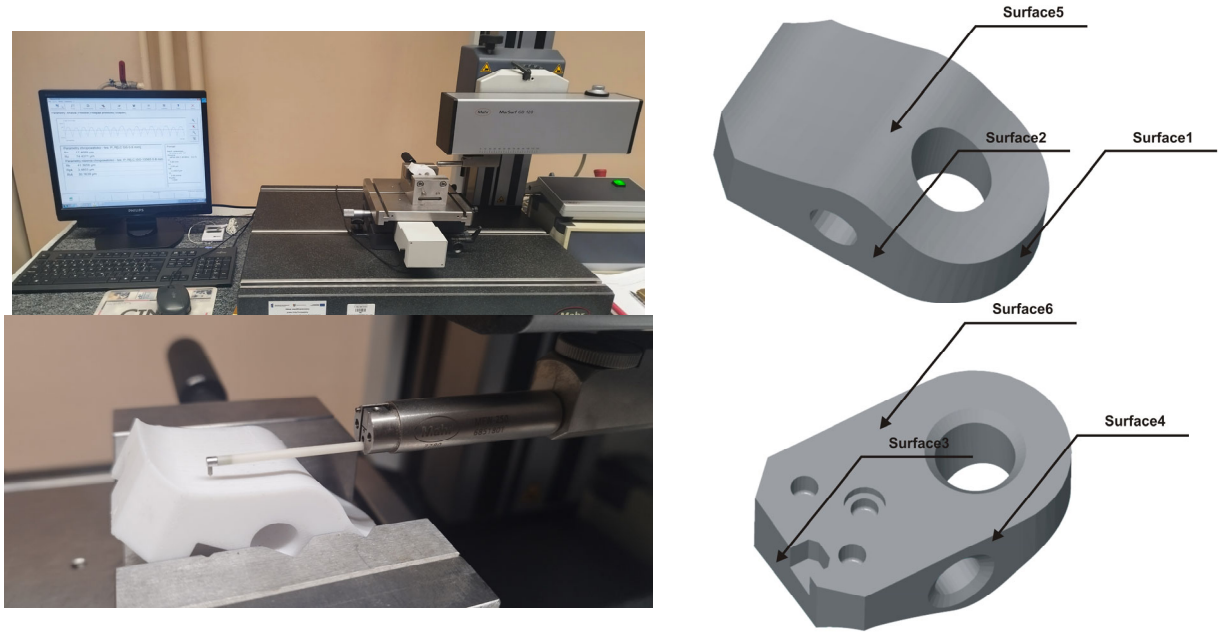
the PC-10 material, the models were coated with an anti-reflective powder before measurement. Additionally, markers were placed on the models to ensure a more accurate alignment of individual scans.

**Table 1.** Established measurement parameters for the GOM Scan 1.

| Parameters | Value |
|---|---|
| Pixel resolutions cameras | 5,000,000 |
| Measuring area | 200 mm × 125 mm × 450 mm |
| Min. point resolution | 0.060 mm |
| Number of points per scan | 5,000,000 |
| Number of rotations of the measuring table | 13 |

The measurements were conducted using two different model orientations. Each measurement series at a specific orientation included 13 scans taken at various angles on the measuring table. The two scans from each series were then merged. Initially, we performed a basic alignment using markers placed on the object. This was followed by a more precise alignment using the *best-fit* method. As a result, we obtained a single scan that combined the two measurement series. The average alignment deviation across all models was 0.019 mm.

The MarSurf XR 20 system with drive unit MarSurf GD 120 was used in the surface roughness measurement process (Figure 3a). This system uses horizontal scanning to acquire points arranged according to a line. Scanning is carried out in the *x*-axis. The system calibration process utilizes a D-type standard, which controls the overall instrument calibration. This standard is known for its periodic surface structure, similar to additive manufacturing models. The measurement process of manufactured models was carried out on six surfaces (Figure 3b). On each surface, three measurements were taken in the direction perpendicular to the prevailing irregularities. Measurement parameters are shown in Table 2.




(**a**) (**b**)

**Figure 3.** Measurement of the surface roughness of manufactured test models: (**a**) Measuring station; (**b**) marked measuring area.

**Table 2.** Established measurement parameters for the MarSurf XR 20 with MarSurf GD 120.

| Parameters | Value |
|---|---|
| Measuring range | ±250 µm |
| Vertical resolution | 5 nm |
| Sampling distance | 0.5 µm |
| Measuring speed | 0.5 mm/s |
| Radius of measuring probe's tip | 2 µm |
| Cut-off length—surfaces in contact with support | 2.5 mm |
| Cut-off length—other surfaces | 0.8 mm |

## 3. Results

### *3.1. Analysis of 3D Deviations and Inspection Sections*

The research involved verifying the dimensional and geometrical accuracy of models manufactured in five different orientations. The GOM Inspect 2019 software from Zeiss was used to verify the geometrical accuracy. The alignment of the nominal model, which was obtained during the CAD design stage and with the reference model measured using the GOM Scan 1 optical system, was conducted using the best-fit method. The average alignment error for this method was approximately 0.05 mm. Based on the results, three-dimensional deviation maps were generated (Figure 4), and statistical parameters (based on all valid points) were compiled and are presented in Table 3. In addition, Figures 5–9 present an inspection section for all model orientations in 3D printer space.

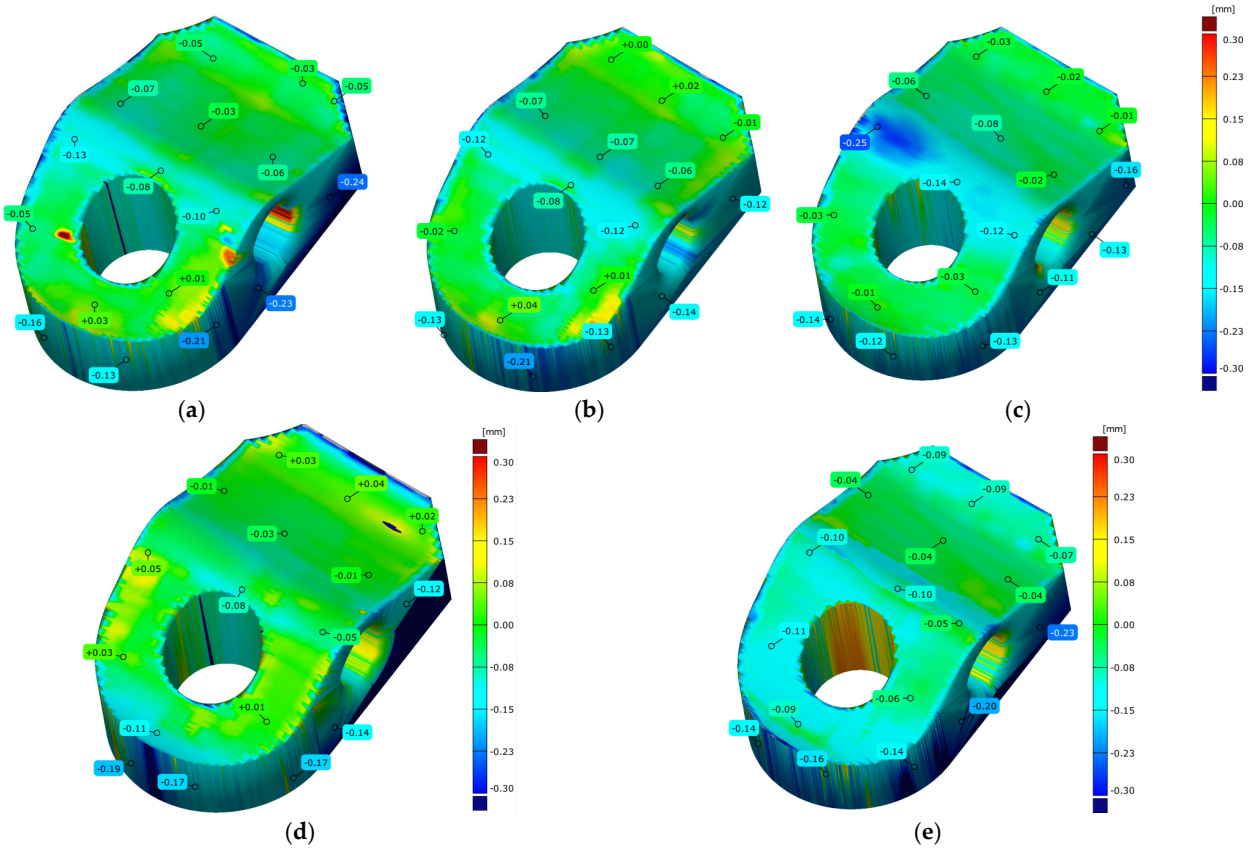



**Figure 4.** Three-dimensional deviation maps for orientations in the 3D printer space: (**a**) 1; (**b**) 2; (**c**) 3; (**d**) 4; (**e**) 5.

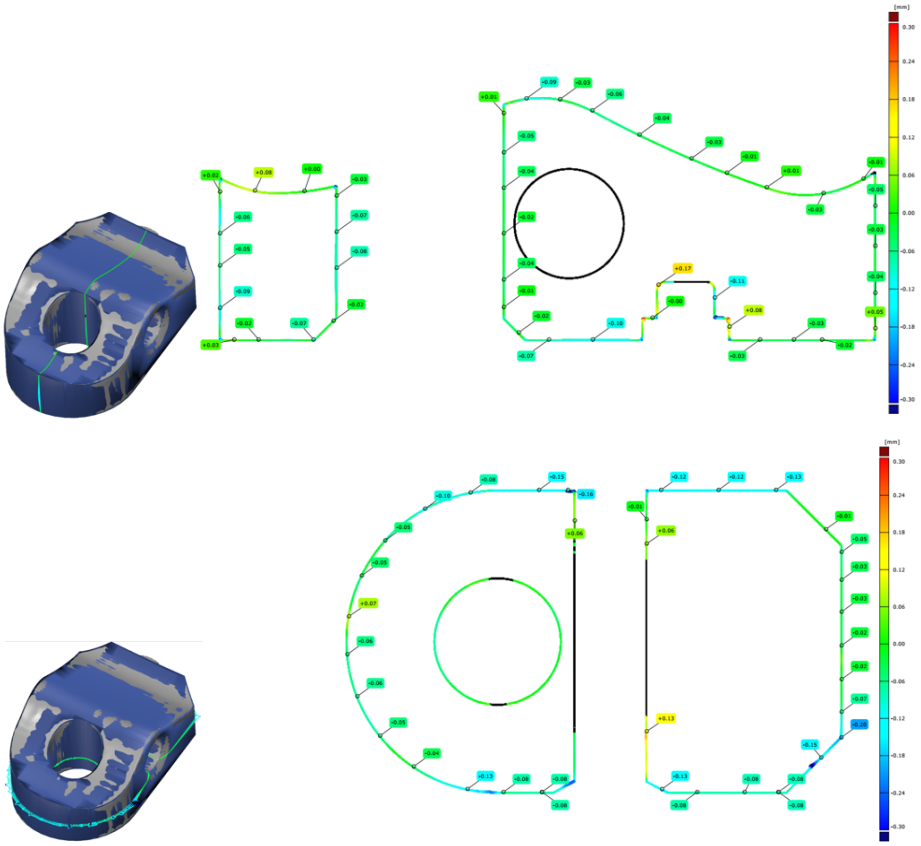


**Figure 5.** Inspection section for the first orientation in the 3D printer space.

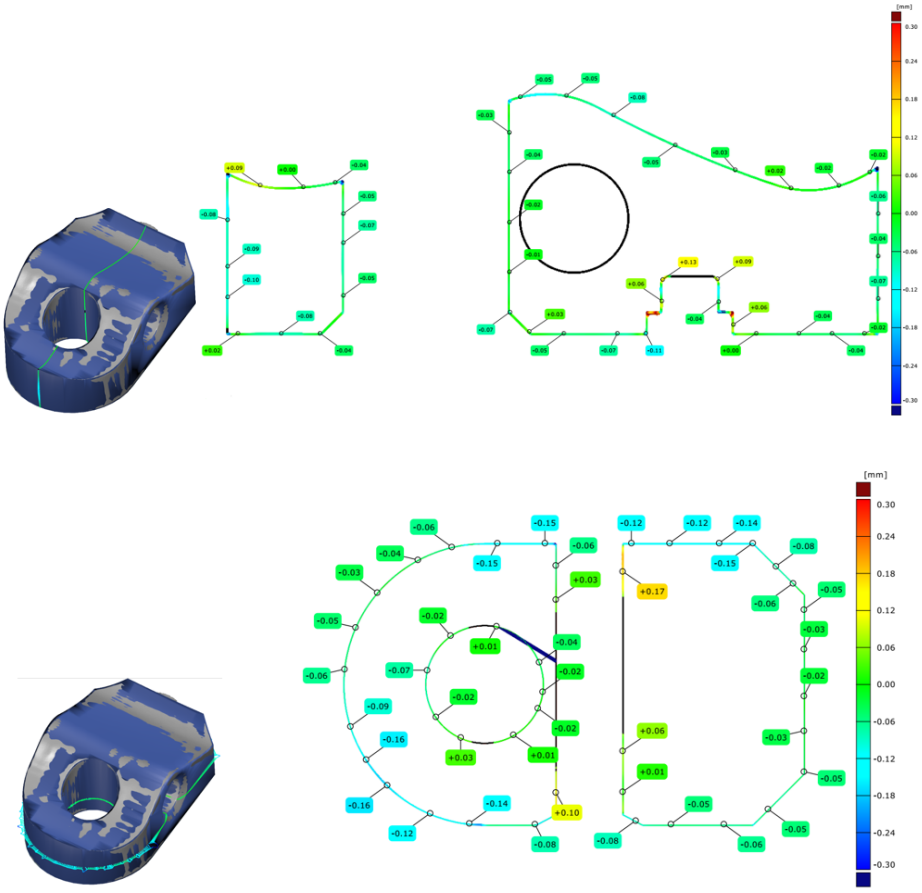


**Figure 6.** Inspection section for the second orientation in the 3D printer space.

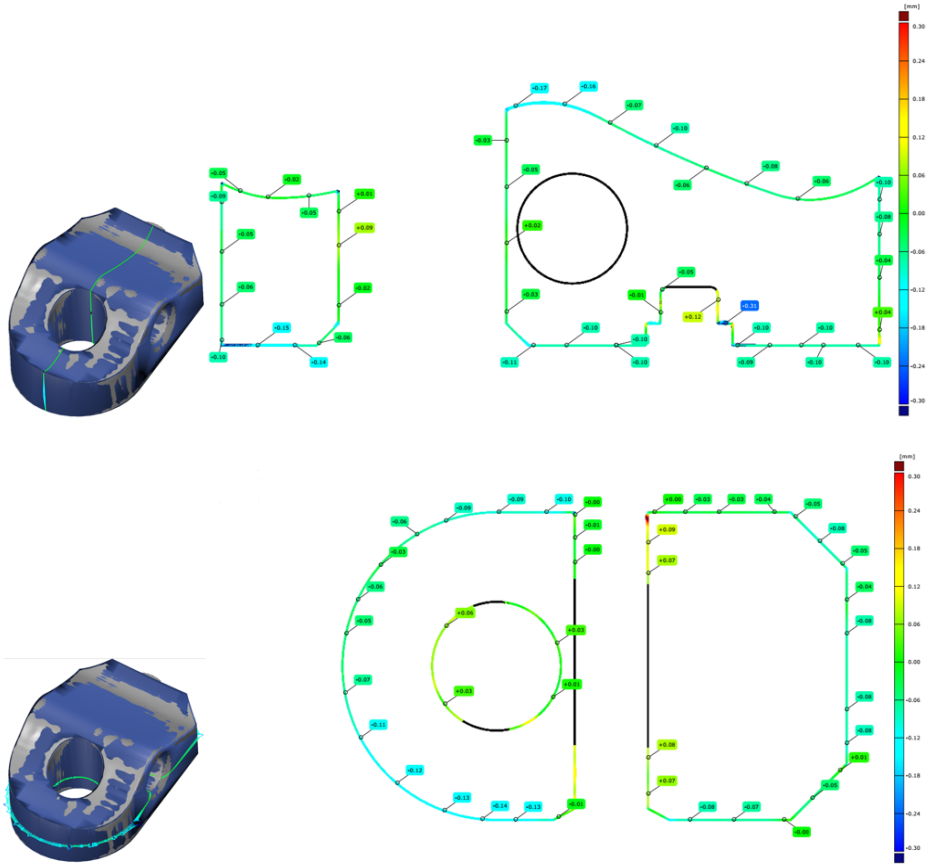


**Figure 7.** Inspection section for the third orientation in the 3D printer space.

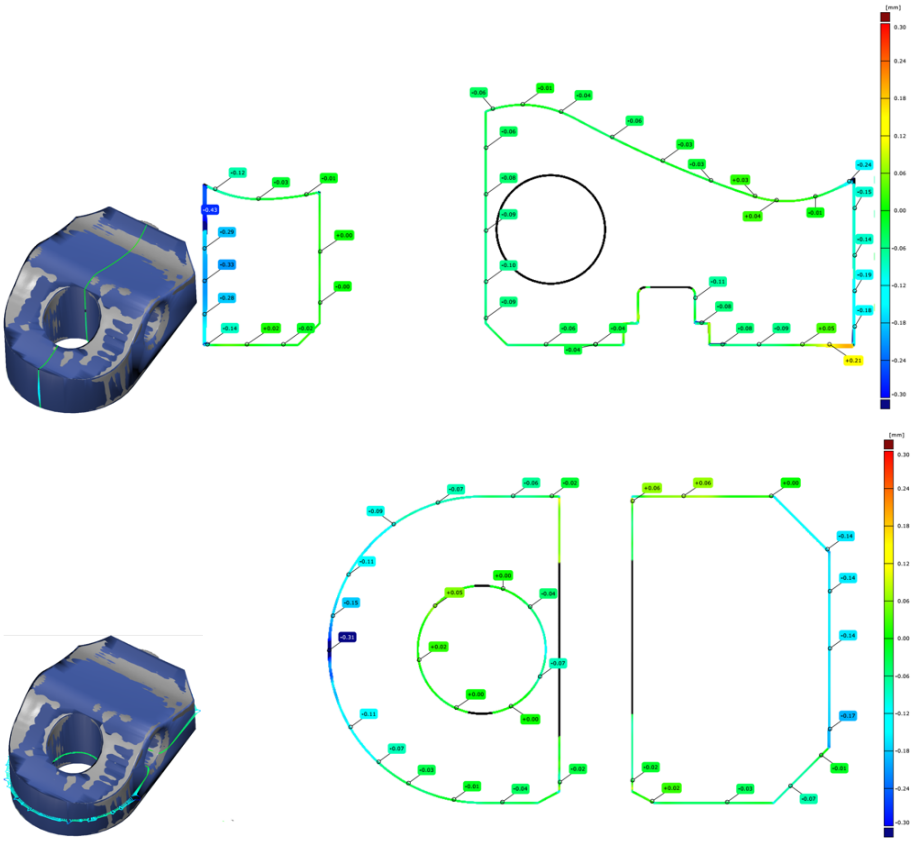


**Figure 8.** Inspection section for the fourth orientation in the 3D printer space.

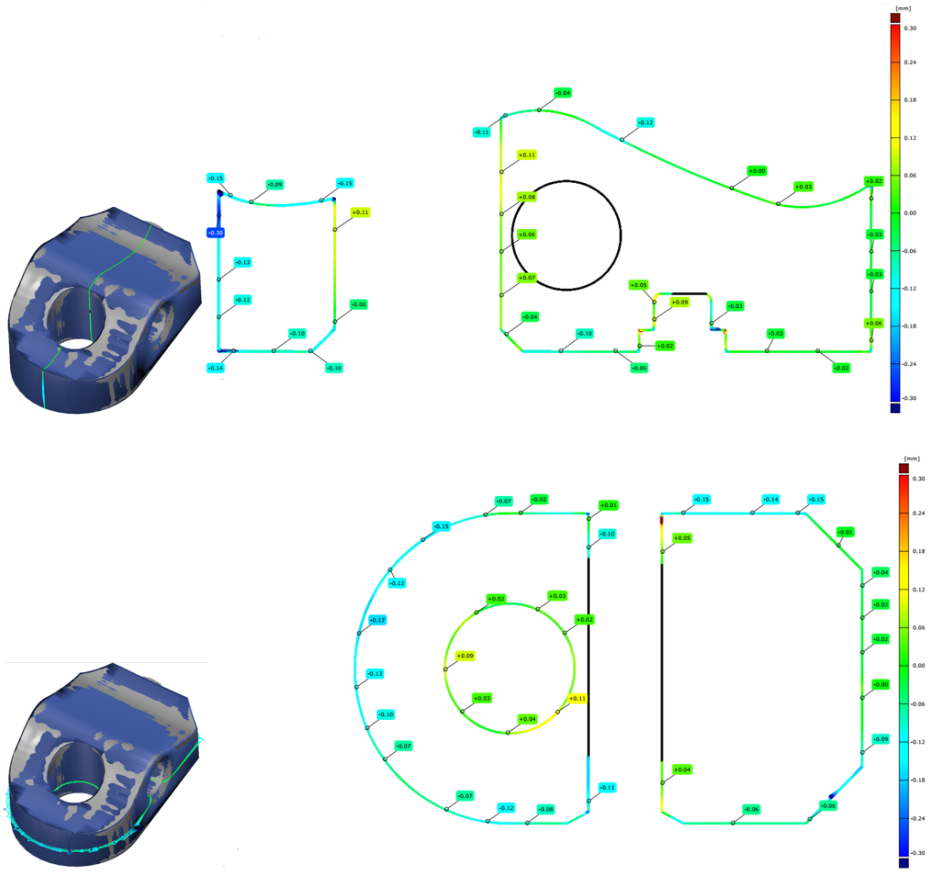


**Figure 9.** Inspection section for the fifth orientation in the 3D printer space.

**Table 3.** Averaged results assessing geometrical accuracy.

| Parameters | Orientation Number | | | | |
|---|---|---|---|---|---|
| | **1** | **2** | **3** | **4** | **5** |
| **Number of valid points** | 54,331 | 49,229 | 44,792 | 50,927 | 50,525 |
| **Maximum deviation ($y_{max}$) [mm]** | 0.560 | 0.461 | 0.507 | 0.564 | 0.407 |
| **Minimum deviation ($y_{min}$) [mm]** | −0.505 | −0.461 | −0.465 | −0.592 | −0.485 |
| **Range ($R$) [mm]** | 1.065 | 0.957 | 0.972 | 1.156 | 0.892 |
| **Mean deviation ($y_{mean}$) [mm]** | −0.080 | −0.077 | −0.100 | −0.056 | −0.060 |
| **Standard deviation ($\sigma$) [mm]** | 0.162 | 0.148 | 0.154 | 0.156 | 0.150 |

The average value of local deviations (3D deviations) $y_{mean}$ for all models was negative. This indicates the dominance of negative deviations on the model. The average value of deviations in the models varied from −0.056 mm (for model 4) to −0.100 mm (for model 3). The difference between the extreme observed $y_{mean}$ values was almost double. The mean $y_{mean}$ value was −0.075 mm and the standard deviation σ was 0.018 mm. To present variability of $y_{mean}$ and σ across all models (with different orientations), the coefficient of variation (VC = standard deviation/ | mean | ) was calculated. The coefficient of variation has the advantage, compared with other parameters describing variability (e.g., spread, standard deviation, variance), that its value does not depend on the unit in which the

variable is expressed. It also indicates how large the variability is in relation to the average value. The coefficient of variation of $y_{mean}$ values was 24%. Models printed in orientations 4 and 5 had a $y_{mean}$ smaller than the mean. All models had a similar standard deviation of local deviations, indicating consistent variability. The standard deviation varied in the range of 0.148–0.162 mm. The coefficient of variation of the standard deviation σ was only 3.5%.

As part of the study, the following geometrical accuracy parameters were determined:

- Maximum ($y_{max}$) and minimum ($y_{min}$) deviations.
- Range ($R$), which is defined as the difference between the maximum and minimum values of the deviation (1), as follows:

$$R = y_{max} - y_{min}, \tag{1}$$

- Mean deviation ($y_{mean}$), which is determined by Equation (2), as follows:

$$y_{average} = \frac{1}{n}\sum_{i=1}^{n} y_i \tag{2}$$

- Standard deviation ($\sigma$), which is determined by Equation (3), as follows:

$$\sigma = \frac{1}{(n-1)}\sqrt{\sum_{i=1}^{n}(y_i - y_{mean})^2}, \tag{3}$$

### *3.2. Analysis of Deviations of Linear Dimensions and Geometric Deviations*

After comparing the 3D deviations, the selected linear dimensions were determined based on the Gauss fitting criterion. Geometric characteristics were analyzed in two groups: characteristics that do not need a base (form deviations) and characteristics with base (orientation and position deviations). All measured characteristics are presented in Figure 10.

The following linear dimensions were chosen during the evaluation process:

- No. 1—model length: 67.5 mm;
- No. 2—model width: 41.25 mm;
- No. 3—model height at the highest point: 27.974 mm;
- No. 4—hole diameter: ∅ 17.25 mm;
- No. 5—hole diameter: ∅ 11.25 mm;
- No. 6—hole diameter: ∅ 9 mm;
- No. 7—depth of socket no. 1: 6 mm;
- No. 8—depth of socket no. 2: 6 mm;
- No. 9—width of socket no. 1: (8.25 mm wide);
- No. 10—width no. of socket 2: (10.5 mm wide).

The effect of model orientation on linear dimension deviations was examined using analysis of variance for repeated measurements, with deviation number as the subject and a significance level of 0.05. The analysis was performed using JMP 12.0 software (SAS Institute Inc., Cary, NC, USA). It showed no statistical difference between the groups, i.e., between the values of deviations acquired for models produced in different orientations. This indicates that the model's orientation did not affect deviation values in the tests conducted. The $p$-values determined by the analysis of variance for linear deviations were 0.11.

The values of deviations of linear dimensions were negative in most cases (Figure 11, Table 4). This corresponds to the dominance of local deviations with negative signs on all models. The largest negative deviations were associated with model size characteristics (Nos. 1–3). The magnitude of the deviation was found to be independent of the relationship between the characteristic and the printer axis. For dimension Nos. 1–3, the average value

of the absolute deviation (considering all orientations) was 0.30 mm, and for the other dimensions it was 0.07 mm. A proportion of 50% of the middle values of linear deviations (between quantiles 1 and 3) were in the range of between −0.13 mm and 0.05 mm. The average value of absolute deviations depending on the orientation varied in the range of 0.09–0.26 mm and was highest for model 5.

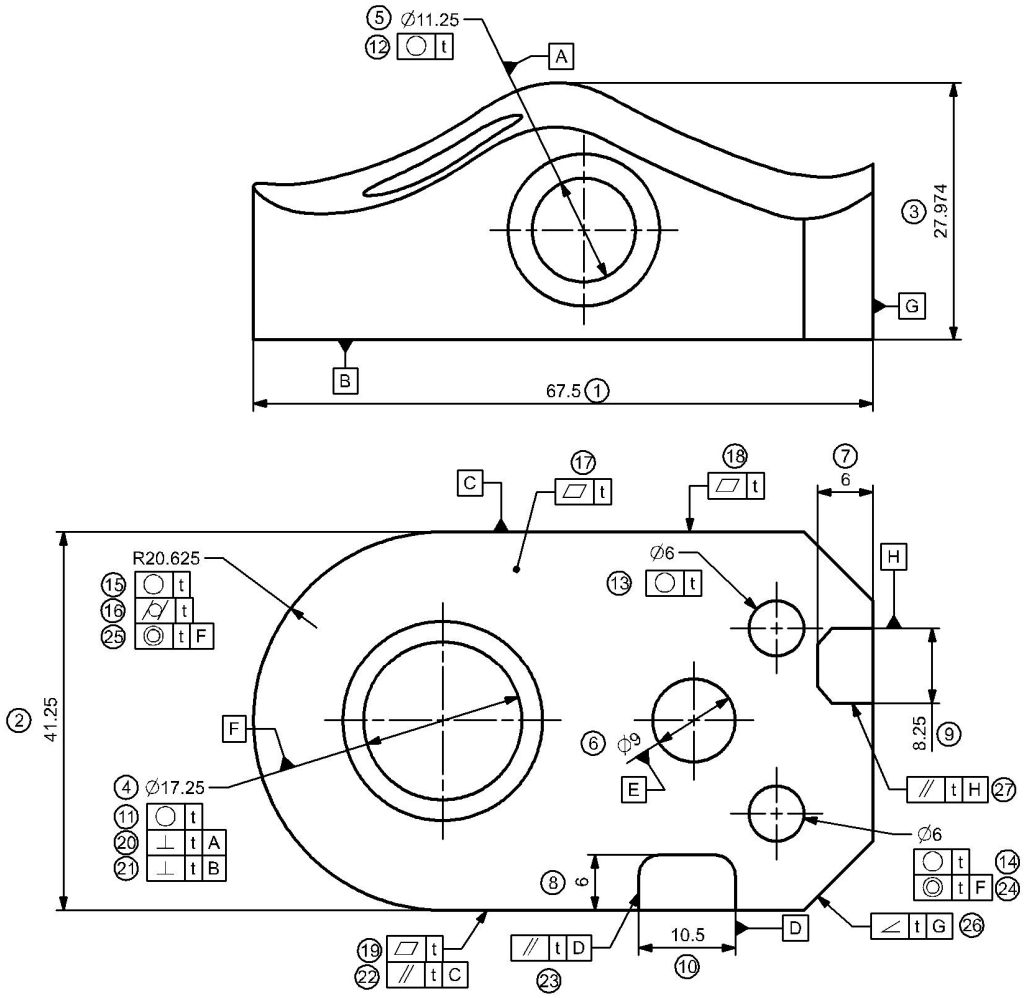



**Figure 10.** Measured characteristics.

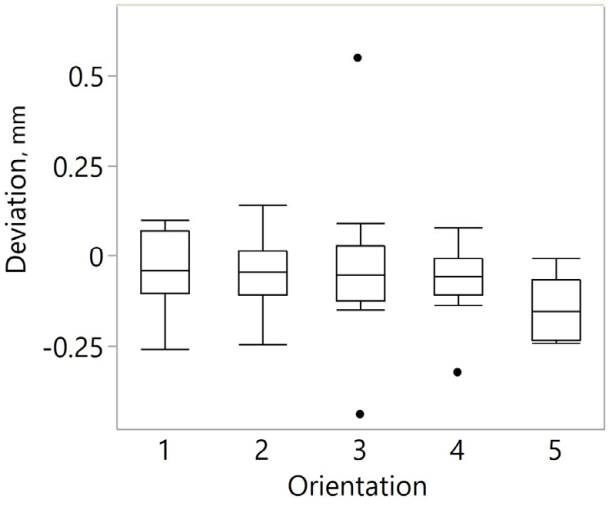



**Figure 11.** Deviations of linear dimensions regarding model orientation.

**Table 4.** Basic statistics of deviations of linear dimensions regarding model orientation.

| Orientation | Dev. of Linear Dimension, mm | | | | | Absolute Dev. of Linear Dimension, mm | | | | |
|---|---|---|---|---|---|---|---|---|---|---|
| | **Mean** | **Median** | **Std Dev** | **Min** | **Max** | **Mean** | **Median** | **Std Dev** | **Min** | **Max** |
| 1 | −0.04 | −0.04 | 0.12 | −0.26 | 0.10 | 0.10 | 0.07 | 0.08 | 0.02 | 0.26 |
| 2 | −0.06 | −0.05 | 0.11 | −0.25 | 0.14 | 0.09 | 0.06 | 0.09 | 0.01 | 0.25 |
| 3 | −0.03 | −0.06 | 0.25 | −0.44 | 0.55 | 0.16 | 0.08 | 0.18 | 0.01 | 0.55 |
| 4 | −0.07 | −0.06 | 0.11 | −0.33 | 0.08 | 0.09 | 0.08 | 0.09 | 0.02 | 0.33 |
| 5 | −0.26 | −0.16 | 0.37 | −1.17 | −0.01 | 0.26 | 0.16 | 0.37 | 0.01 | 1.17 |

In the process of verifying the accuracy of the manufacturing of the model using the additive FDM technique, a study was carried out to determine the following basic form deviations:

- No. 11—roundness deviation of a hole ø 17.25 mm;
- No. 12—roundness deviation of a hole ø 11.25 mm;
- No. 13—roundness deviation of a hole ø 6 mm;
- No. 14—roundness deviation of a hole ø 6 mm;
- No. 15—roundness deviation of radius 20.625;
- No. 16—cylindricity deviation of radius 20.625;
- No. 17—surface flatness deviation;
- No. 18—surface flatness deviation;
- No. 19—surface flatness deviation.

In the next step, the following orientation and position deviations were evaluated:

- No. 20—perpendicularity tolerance of an axis of a hole ∅ 17.25 mm (20) related to a datum axis of a hole ∅ 11.25 mm (base A);
- No. 21—perpendicularity tolerance of an axis of a hole ∅ 17.25 mm (21) related to a datum plane (base A);
- No. 22—parallelism tolerance of a surface (22) related to a datum plane (base C);
- No. 23—parallelism tolerance of a surface (23) related to a datum plane (base D);
- No. 24—coaxiality tolerance of an axis of a hole ∅ 6 mm (24) related to a datum axis of a hole ∅ 9 mm (base E);
- No. 25—coaxiality tolerance of an axis of a hole ∅ 20,625 mm (25) related to a datum axis of a hole ∅ 17.25 mm (base F);
- No. 26—angularity tolerance of a surface (26) related to a datum plane (base G);
- No. 27—parallelism tolerance of a surface (27) related to a datum plane (base H).

The effect of model orientation on deviation values was examined using analysis of variance for repeated measurements. Analyses were carried out separately for form deviations and other groups of deviations. They showed no statistical difference between the groups—between the values of deviations acquired for models produced in different orientations. This means that, in the tests conducted, the orientation of the model did not affect the value of deviations. The *p*-value for form deviation was 0.58, and for orientation and position deviation, it was 0.76.

The average value of orientation and position deviations for each model varied in the range of 0.15–0.20 mm, and for form deviation varied in a similar range, i.e., 0.16–0.20 mm (Figure 12, Table 5). A proportion of 50% of the middle values of form deviations were in the range of 0.15–0.22 mm, and, of orientation and position deviations, were in the range of 0.07–0.24 mm.

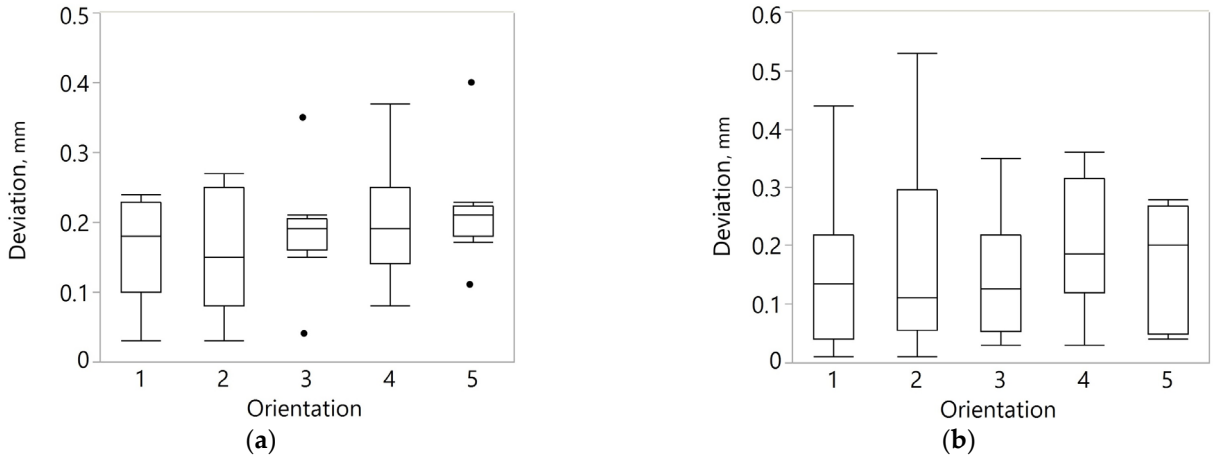



**Figure 12.** Deviations of various types regarding model orientation: (**a**) Form deviations; (**b**) orientation and position deviations.

**Table 5.** Basic statistics of form deviations as well as orientation and position deviations regarding model orientation.

| Orientation | Form Deviation, mm | | | | | Orientation and Position Dev., mm | | | | |
|---|---|---|---|---|---|---|---|---|---|---|
| | Mean | Median | Std Dev | Min | Max | Mean | Median | Std Dev | Min | Max |
| 1 | 0.17 | 0.18 | 0.08 | 0.03 | 0.24 | 0.15 | 0.14 | 0.14 | 0.01 | 0.44 |
| 2 | 0.16 | 0.15 | 0.09 | 0.03 | 0.27 | 0.17 | 0.11 | 0.18 | 0.01 | 0.53 |
| 3 | 0.19 | 0.19 | 0.08 | 0.04 | 0.35 | 0.15 | 0.13 | 0.11 | 0.03 | 0.35 |
| 4 | 0.20 | 0.19 | 0.09 | 0.08 | 0.37 | 0.20 | 0.19 | 0.11 | 0.03 | 0.36 |
| 5 | 0.21 | 0.21 | 0.08 | 0.11 | 0.40 | 0.18 | 0.20 | 0.10 | 0.04 | 0.28 |

### *3.3. Analysis of Surface Roughness*

As part of the study, the following surface roughness parameters were determined:

- Arithmetical mean height (*Ra*) indicates the average of the absolute value along the sampling length (4):

$$R_a = \frac{1}{lr}\int_0^{lr} |Z(x)|dx, \tag{4}$$

- Maximum height of the profile (*Rz*) indicates the absolute vertical distance between the maximum profile peak height (*Rp*) and the maximum profile valley depth (*Rv*) along the sampling length (5):

$$R_z = R_p + R_v \tag{5}$$

During visual inspection, it was possible to distinguish three types of surfaces on the models: the surfaces formed by the deposition of the last layer (denoted hereafter as *last-layer*), the surfaces attached to the support (denoted hereafter as *support-adjacent*), and the remaining surface, on which the successive layers laid down were clearly distinguishable (denoted as *layer-type*) (Figure 13). Orientation influenced the presence of surface types and the roughness parameters on a given surface (Figure 14).

The results of the measurement of *Ra* and *Rz* parameters were found to show significant differences in the values of these parameters depending on the type of surface (Figure 15, Table 6). The surfaces that represented the last layer of the model had the lowest roughness (expressed by *Ra* and *Rz*). These had a periodic character and were the glossiest when compared with the other surfaces. The average value of the *Ra* parameter on them

was 3.77 µm. The surfaces adjacent to the support had the most isotropic character and were the most matte. The average value of the *Ra* parameter was 9.47 µm, which was about 2.5 times higher than on the *last-layer* type surfaces. The remaining surfaces were clearly distinguished by the successive layers laid down, hence their character was also periodic. The average value of the *Ra* parameter was the highest in their case, at 14.07 µm, which was more than 3.5 times higher than that of the smoothest surfaces.

Because the *last-layer* and *support-adjacent* type surfaces occurred only once in a given orientation or were absent, and were clearly different from the prevailing *layer-type* surfaces on the model, the study of the effect of orientation on *Ra* and *Rz* parameters was carried out considering only the *layer-type* surfaces. The average value of *Ra* and *Rz* parameters of models printed in orientations 1–4 are similar (Figure 16, Table 7). The *Ra* parameter varies in the range of 12.7–13.8 µm, and *Rz* in the range of 57.2–61.2 µm. Higher average values of roughness parameters were observed for the model printed in orientation 5. However, the average *Ra* value for the model in orientation 5 was 17.21 µm, and Rz was 71.26 µm.

**Table 6.** Roughness parameters depending on surface type.

| Surface Type | *Ra*, µm | | | *Rz*, µm | | |
|---|---|---|---|---|---|---|
| | **Mean** | **Median** | **Std Dev** | **Mean** | **Median** | **Std Dev** |
| Last | 3.77 | 3.62 | 1.13 | 22.41 | 23.58 | 4.11 |
| Support | 9.47 | 9.01 | 1.33 | 53.70 | 53.85 | 8.40 |
| Layers | 14.07 | 12.45 | 3.40 | 62.56 | 57.53 | 12.36 |

**Table 7.** Roughness parameters depending on orientation.

| Orientation | *Ra*, µm | | | *Rz*, µm | | |
|---|---|---|---|---|---|---|
| | **Mean** | **Median** | **Std Dev** | **Mean** | **Median** | **Std Dev** |
| 1 | 12.81 | 12.45 | 1.86 | 57.23 | 57.47 | 8.00 |
| 2 | 13.77 | 12.51 | 2.98 | 61.19 | 57.96 | 12.13 |
| 3 | 12.70 | 12.14 | 1.72 | 60.28 | 56.66 | 10.86 |
| 4 | 12.93 | 12.03 | 2.40 | 59.78 | 58.13 | 8.47 |
| 5 | 17.21 | 17.67 | 4.33 | 71.26 | 71.88 | 15.25 |

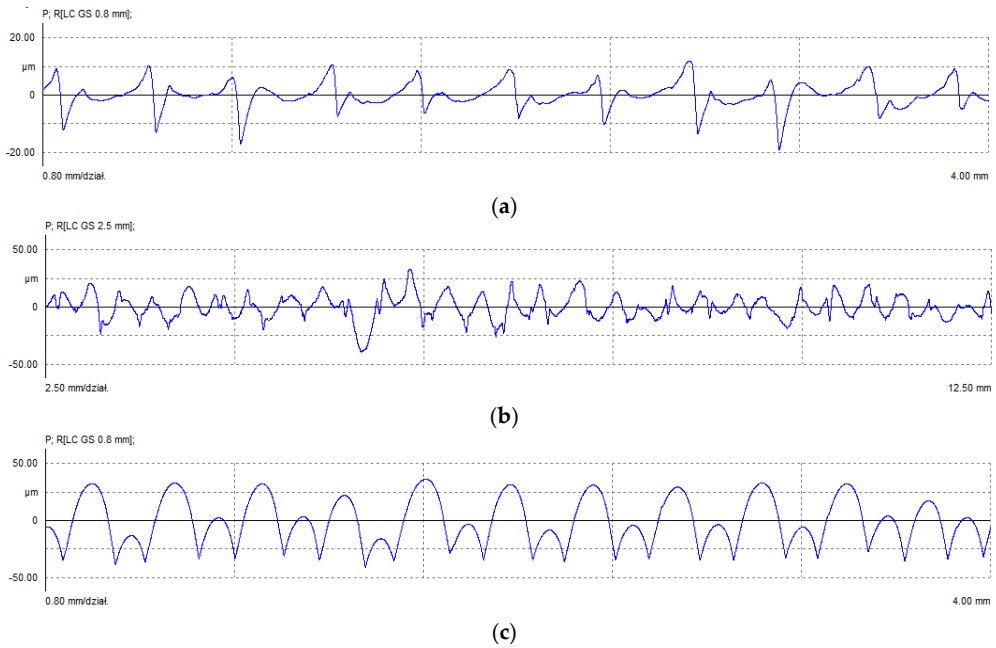



**Figure 13.** Examples of surface roughness profiles of various types: (**a**) *Last-layer*; (**b**) *support-adjacent;* (**c**) *layer-type*.

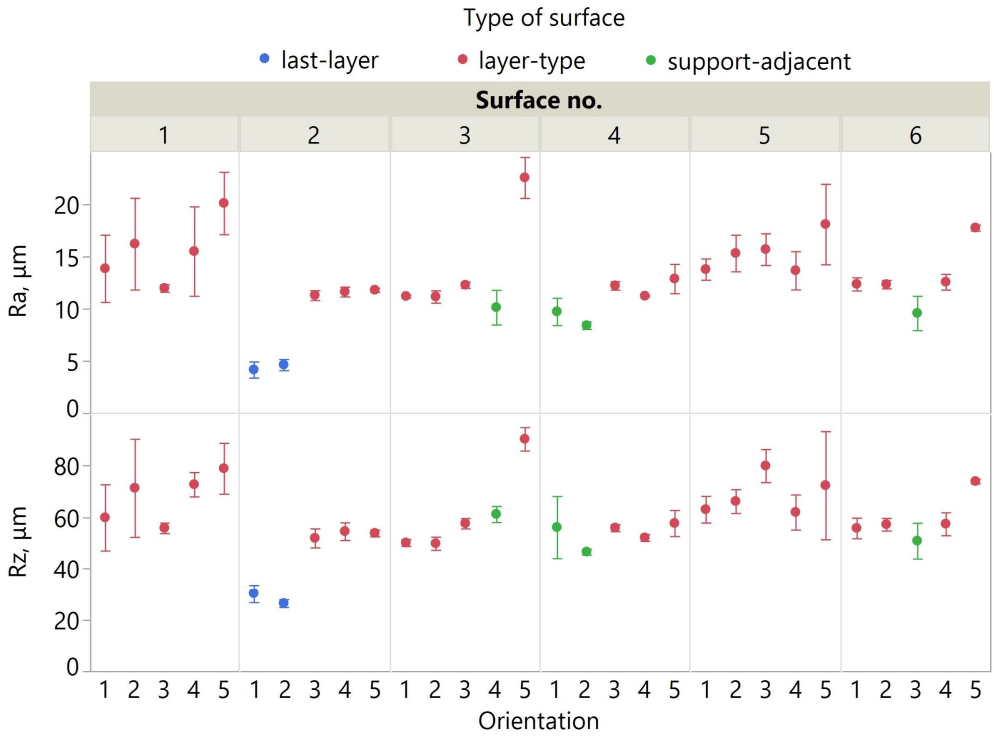



**Figure 14.** Surface roughness parameters regarding model orientation and surface type.

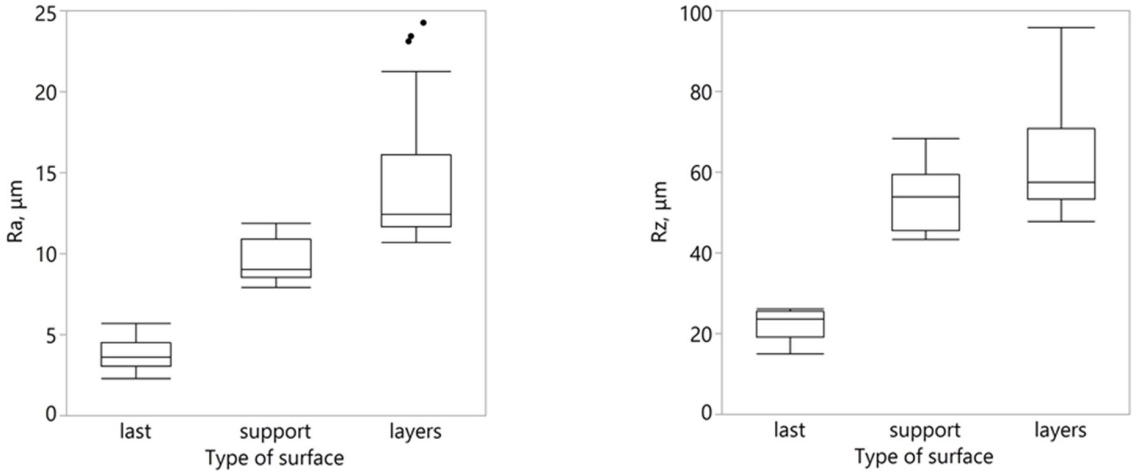



**Figure 15.** Boxplots of roughness parameters depending on surface type.

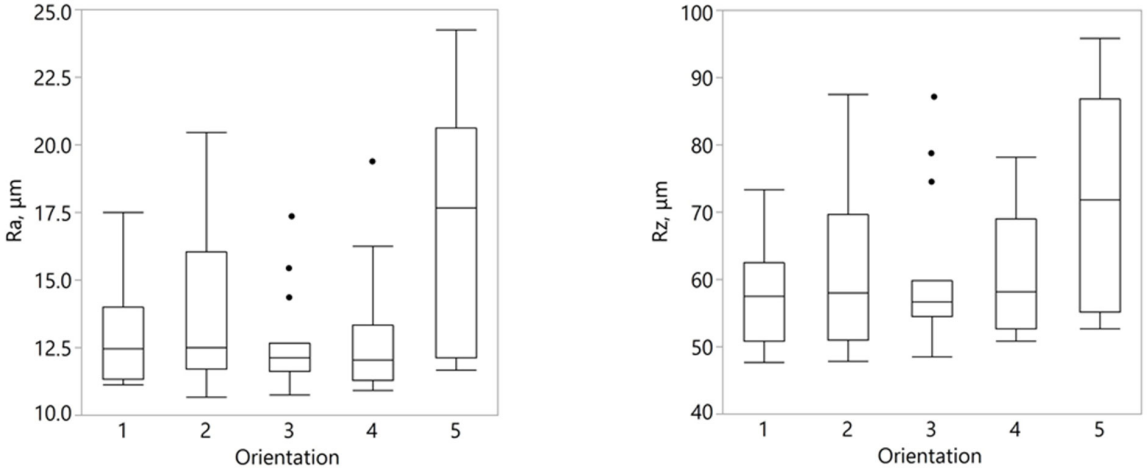



**Figure 16.** Boxplots of roughness parameters depending on orientation.

## 4. Discussion

Polycarbonates are a particularly interesting material in terms of their physical and mechanical properties [41]. They are characterized by high resistance to the destructive influence of various mechanical factors. Polycarbonates are hard polymers, and hardness is one of the factors that gives these plastics good mechanical strength [42]. Polycarbonates also exhibit very good impact strength. They are, therefore, highly resistant to the potentially destructive effects of dynamic loading [43]. As a result, polycarbonates are most often used to manufacture additive models for the aerospace industry in the production of short carbon microfibers [43], the automotive industry in the production of door panels and wheel boxes [44], and medical industries in the production of intervertebral lumbar cages [45]. Additive methods are now increasingly being used to manufacture tools in the form of molds for the aerospace industry, among other industries. Manufacturing molds from polymeric material allow for a significant reduction in costs and the time required for the production process, when compared with traditional machining methods [46]. This is of great importance among companies involved in producing machine parts and equipment, as it allows them to respond dynamically to changes in customer demand. Unfortunately, most models made from polymeric materials are characterized by a surface finish that is not of high quality, which limits the applicability of 3D printed models for direct and indirect use, e.g., model kits for producing molds for short production series [47]. Therefore, in the case of the incremental manufacture of models using polymeric materials, it is often necessary to carry out further surface finishing. This involves, among other things, usually costly mechanical or chemical treatment. To limit the applicability of finishing, it is necessary to develop guidelines at the stage of selecting manufacture parameters, e.g., the model's orientation in the 3D printer space, minimizing geometric deviations and surface roughness.

### *4.1. Dimensional and Geometric Assessment*

Due to the good mechanical properties of the PC material, it is important to also pay attention to the metrological evaluation of the models made from this type of polymer material. The literature review of the metrological tests carried out on models made on the Fortus 360-mc 3D printer mainly concern dimensional evaluation and geometry accuracy. Meanwhile, the dimensional deviation studies by Stratasys show that models characterized by regular shapes are within $\pm$0.13 mm. However, the study did not concern the PC-10 material, but the ABS-M30 material, and the layer thickness was 0.25 mm [48]. In the case of assessing the geometry accuracy, a study conducted on the PC-10 material was observed in the literature. The models were made with an applied layer thickness of 0.178 mm. The deviations obtained varied from $\pm$0.188 mm to $\pm$0.3 mm [25]. The variability in the results was due to the use of different measurement systems to digitize the geometry of the mandibular anatomical structures. A more extensive analysis of the problem focuses on studies involving PC-material models and other types of 3D printers. In [49], research was conducted to examine the effects of varying layer thickness and manufacturing temperature on the resulting dimensional deviations. The findings indicate that increasing the temperature and reducing the layer thickness decreases the maximum values of linear deviations. Specifically, the maximum deviation documented was 0.083 mm, while the minimum was 0.018 mm. Additionally, this research was noted in [50]. In this publication, linear dimensions were evaluated on a manufactured model of a cranial vault defect. The averaged results were found to show that the deviation values were within $\pm$0.09 mm. This analysis was conducted using measurements obtained from micro-CT scans. However, the article's authors did not specify the layer thickness used for manufacturing the model. More extensive studies have been conducted, as detailed

in [51,52], focusing on assessing geometry accuracy. Ref. [51] measured the geometry using a micro-CT scanner. The resulting three-dimensional deviation map indicated that the deviations of the ship's view model, created with a layer thickness of 0.25 mm, were within ±0.3 mm. Similar findings are reported in [52,53]. The first study used a 3D optical scanner to digitize the geometry, while the second used a micro-CT scanner. In [54], the authors included research regarding how changing the orientation of 3D models affects their geometric accuracy. The authors also studied the impact of different types of support materials and layer thicknesses. The tests focused on cylindrical geometries in order to evaluate dimensional accuracy and selected geometric deviations. Measurements were conducted using a coordinate measuring machine (CMM). The publication highlights that changing the orientation significantly affects the accuracy of the model geometry. Specifically, the most favorable orientation for the specimens was along the *Z*-axis, which also helped reduce the amount of support material needed during manufacturing. However, the authors emphasize the need for further research, as only one linear dimension and four geometric deviations were evaluated in their tests. The study presents a notable extension of research compared with previously published articles. The authors focused on measuring linear deviations along the X, Y, and Z axes. The standard deviation for orientations 1, 2, and 4 was approximately 0.1 mm, comparable to the publication findings [50]. However, orientations 3 and 5 significantly increased the standard deviation, reaching values greater than 0.2 mm and nearly 0.4 mm, respectively. This increase may be related to the longer manufacturing time of the model, which likely resulted in a more significant influence from the shrinkage of the PC material used for the model. In addition, attention was paid to form deviations, e.g., roundness, cylindricity, and flatness errors. Comparable results were obtained in each model orientation. The standard deviation value was approximately 0.1 mm. In [54], higher deviation values were observed. The increase in values may be related to the use of a different digitization method. Considering the analysis of the obtained orientation and position deviations, most are within ±0.2 mm. Most geometrical deviations are within ±0.3 mm, confirming the results obtained in publications [25,51].

### *4.2. Surface Roughness Assessment*

Contact and optical methods are used in the surface roughness assessment process. However, the procedures for the profile contact method are most regulated. All rules and guidelines for evaluating the surface texture with this method are contained in ISO 21920 [37–39]. This fact considerably facilitates surface roughness testing concerning optical methods, for which new measurement guidelines are continuously being developed. Several studies on the evaluation of surface roughness parameters of samples made with additive techniques using 2D [54,55] and 3D [56,57] profile methods can be observed in the literature. The investigation of the surface texture condition of models made by MEX methods is significant for the sake of its anisotropic surface properties [58]. The literature review indicates that there are studies focused on evaluating surface roughness when the orientation of a model is changed in the 3D printing process. However, these studies primarily focus on materials such as PLA [58–60] and ABS [61]. Some publications also investigate the surface roughness of a PC material [62,63]. It is important to note that these measurements were conducted only along the overlap of the layers and did not account for the effects of changing the model's orientation within the 3D printer space. Refs. [62,63] investigated roughness parameters on a single profile. In the case of the first publication, the averaged Ra parameter was 3.5826 µm; in the second publication, this was 7.39 µm. In [64], 3D roughness parameters were investigated. The measured results show that the average value of the Sa parameter was 12.87 µm. The results may be due to different manufacturing parameters (e.g., different layer thicknesses were used) and

various measuring tools. In the case of the results presented in the current publication, the most consistent results were obtained in [64]. The averaged values for the Ra parameter were mostly in the range of approximately 13 μm. Only when the test model was made at an angle of 45 degrees was the averaged value for the Ra parameter above 17 μm. This may be related to the complicated model manufacturing process in this orientation.

## 5. Conclusions

The study examines models manufactured using FDM technology in five orientations, utilizing polycarbonate (PC) material and a FORTUS 360mc printer. The models featured both simple geometries (planes and cylinders) and complex free-form surfaces. Their accuracy was evaluated with a GOM Scan 1 scanner and GOM Inspect 2019 software, focusing on 3D deviations as well as dimensional and geometric deviations (form, position, and orientation). Surface roughness was measured using a MarSurf XR profilometer, analyzing the Ra and Rz parameters.

The findings can be summarized as follows:

- Predominantly negative 3D deviations were observed across all models, with average deviations $y_{mean}$ ranging from −0.056 mm to −0.100 mm. Variability in 3D deviations was consistent across models, with standard deviations of 0.148–0.162 mm, and was not influenced by model orientation.
- Model orientation had no significant effect on linear deviations. Most linear deviations were negative, with size-related dimensions showing the largest average absolute deviation (0.30 mm), compared with 0.07 mm for other dimensions.
- Geometric deviations, including orientation, position, and form deviations, were not significantly influenced by model orientation. Average orientation and position deviations ranged from 0.15 to 0.20 mm. Form deviations had similar values and ranged from 0.16 to 0.20 mm.
- Surface roughness varied by surface type (*last-layer*, *support-adjacent*, and *layer-type*). Last-layer surfaces exhibited the lowest roughness ($Ra$ = 3.77 μm), support-adjacent surfaces had intermediate roughness ($Ra$ = 9.47 μm), and layer-type surfaces showed the highest roughness ($Ra$ = 14.07 μm). Orientation influenced the presence of surface types and the roughness of layer-type surfaces, with orientations 1–4 showing similar roughness ($Ra$ = 12.7–13.8 μm) and orientation 5 exhibiting the highest roughness ($Ra$ = 17.21 μm).

The lack of the apparent effect of orientation on geometry deviations may be due to the complexity of the model and the analysis of a variety of deviations. This is why further studies should be carried out to determine the effect of model orientation on each particular type of geometric deviation. In order to develop recommendations for the orientation of the model, while taking into account the minimization of deviations, it is necessary to conduct a broader study, properly planned for this specific purpose. The research presented in this paper and future research into determining geometric accuracy and surface roughness may add to the knowledge on developing mold models (with accepted manufacturing accuracy) for producing short-casting series to manufacture components for the aerospace and automotive industries.

**Author Contributions:** Conceptualization, P.T. and A.B.; methodology, P.T. and A.B.; investigation, P.T., A.B. and M.B.; writing—original draft preparation P.T., A.B. and M.B.; writing—review and editing, P.T. and A.B.; visualization, P.T., A.B. and M.B. All authors have read and agreed to the published version of the manuscript.

**Funding:** This research received no external funding.

**Data Availability Statement:** The original contributions presented in the study are included in the article, further inquiries can be directed to the corresponding author.

**Conflicts of Interest:** The authors declare no conflicts of interest.

## References


1. Gao, W.; Zhang, Y.; Ramanujan, D.; Ramani, K.; Chen, Y.; Williams, C.B.; Zavattieri, P.D. The status, challenges, and future of additive manufacturing in engineering. *Comput.-Aided Des.* **2015**, *69*, 65–89. [CrossRef]
2. Ngo, T.D.; Kashani, A.; Imbalzano, G.; Nguyen, K.T.; Hui, D. Additive manufacturing (3D printing): A review of materials, methods, applications and challenges. *Compos. Part B Eng.* **2018**, *143*, 172–196. [CrossRef]
3. Gardan, J. Additive manufacturing technologies: State of the art and trends. In *Additive Manufacturing Handbook*; CRC Press: Boca Raton, FL, USA, 2017; pp. 149–168. [CrossRef]
4. *ISO/ASTM 52900:2021*; Additive Manufacturing—General Principles—Fundamentals and Vocabulary. ISO: Geneva, Switzerland, 2021.
5. *ISO/ASTM 52910:2018*; Additive Manufacturing—Design—Requirements, Guidelines and Recommendations. ISO: Geneva, Switzerland, 2018.
6. Priyadarshi, A.; Shahrani, S.B.; Choma, T.; Zrodowski, L.; Qin, L.; Leung, C.L.A.; Tzanakis, I. New insights into the mechanism of ultrasonic atomization for the production of metal powders in additive manufacturing. *Addit. Manuf.* **2024**, *83*, 104033. [CrossRef]
7. Chu, M.Q.; Wang, L.; Ding, H.Y.; Sun, Z.G. Additive manufacturing for aerospace application. *Appl. Mech. Mater.* **2015**, *798*, 457–461. [CrossRef]
8. Kasatkin, M.M.; Kozhina, T.D.; Federov, M.M. Additive technologies in airplane-engine manufacture. *Russ. Eng. Res.* **2019**, *39*, 262–267. [CrossRef]
9. Böckin, D.; Tillman, A.M. Environmental assessment of additive manufacturing in the automotive industry. *J. Clean. Prod.* **2019**, *226*, 977–987. [CrossRef]
10. Leal, R.; Barreiros, F.M.; Alves, L.; Romeiro, F.; Vasco, J.C.; Santos, M.; Marto, C. Additive manufacturing tooling for the automotive industry. *Int. J. Adv. Manuf. Technol.* **2017**, *92*, 1671–1676. [CrossRef]
11. Ciocca, L.; Mazzoni, S.; Fantini, M.; Persiani, F.; Baldissara, P.; Marchetti, C.; Scotti, R. A CAD/CAM-prototyped anatomical condylar prosthesis connected to a custom-made bone plate to support a fibula free flap. *Med. Biol. Eng. Comput.* **2012**, *50*, 743–749. [CrossRef]
12. Javaid, M.; Haleem, A. Additive manufacturing applications in medical cases: A literature based review. *Alex. J. Med.* **2018**, *54*, 411–422. [CrossRef]
13. Turek, P. Automating the process of designing and manufacturing polymeric models of anatomical structures of mandible with Industry 4.0 convention. *Polimery* **2019**, *64*, 522–529. [CrossRef]
14. Dziubek, T.; Budzik, G.; Kawalec, A.; Dębski, M.; Turek, P.; Oleksy, M.; Cebulski, J. Strength of threaded connections additively produced from polymeric materials. *Polimery* **2022**, *67*, 261–270. [CrossRef]
15. Mao, K.; Greenwood, D.; Ramakrishnan, R.; Goodship, V.; Shrouti, C.; Chetwynd, D.; Langlois, P. The wear resistance improvement of fibre reinforced polymer composite gears. *Wear* **2019**, *426*, 1033–1039. [CrossRef]
16. Vidakis, N.; Petousis, M.; Vaxevanidis, N.; Kechagias, J. Surface roughness investigation of poly-jet 3D printing. *Mathematics* **2020**, *8*, 1758. [CrossRef]
17. Chohan, J.S.; Singh, R. Pre and post processing techniques to improve surface characteristics of FDM parts: A state of art review and future applications. *Rapid Prototyp. J.* **2017**, *23*, 495–513. [CrossRef]
18. Haque, M.E.; Banerjee, D.; Mishra, S.B.; Nanda, B.K. A numerical approach to measure the surface roughness of FDM build part. *Mater. Today Proc.* **2019**, *18*, 5523–5529. [CrossRef]
19. Reddy, V.; Flys, O.; Chaparala, A.; Berrimi, C.E.; Amogh, V.; Rosen, B.G. Study on surface texture of fused deposition modeling. *Procedia Manuf.* **2018**, *25*, 389–396. [CrossRef]
20. Gibson, I.; Rosen, D.; Stucker, B.; Khorasani, M.; Gibson, I.; Rosen, D.; Khorasani, M. Material extrusion. In *Additive Manufacturing*; Springer International Publishing: New York, NY, USA, 2021; pp. 171–201. [CrossRef]
21. Wang, T.M.; Xi, J.T.; Jin, Y. A model research for prototype warp deformation in the FDM process. *Int. J. Adv. Manuf. Technol.* **2007**, *33*, 1087–1096. [CrossRef]
22. Gordon, E.R.; Shokrani, A.; Flynn, J.M.; Goguelin, S.; Barclay, J.; Dhokia, V. A surface modification decision tree to influence design in additive manufacturing. In *Sustainable Design and Manufacturing*; Springer International Publishing: New York, NY, USA, 2016; pp. 423–434. [CrossRef]
23. Srinivasan, R.; Ruban, W.; Deepanraj, A.; Bhuvanesh, R.; Bhuvanesh, T. Efect on infll density on mechanical properties of PETG part fabricated by fused deposition modelling. *Mater. Today Proc.* **2020**, *27*, 1838–1842. [CrossRef]
24. Turek, P.; Budzik, G. Estimating the accuracy of mandible anatomical models manufactured using material extrusion methods. *Polymers* **2021**, *13*, 2271. [CrossRef]

25. Turek, P.; Filip, D.; Przeszłowski, Ł.; Łazorko, A.; Budzik, G.; Snela, S.; Paszkiewicz, A. Manufacturing polymer model of anatomical structures with increased accuracy using cax and am systems for planning orthopedic procedures. *Polymers* **2022**, *14*, 2236. [CrossRef]
26. Lojo, J.M.; Pérez-Barquero, J.A.; Bonmatí, F.G.S.; Agustín-Panadero, R.; Yilmaz, B.; Revilla-León, M. Influence of print orientation on the accuracy (trueness and precision) of diagnostic casts manufactured with a daylight polymer printer. *J. Prosthet. Dent.* **2023**, *132*, 1314–1322. [CrossRef] [PubMed]
27. AlGhamdi, M.A.; Gad, M.M. Impact of Printing Orientation on the Accuracy of Additively Fabricated Denture Base Materials: A Systematic Review. *Dent. J.* **2024**, *12*, 230. [CrossRef] [PubMed]
28. Mantada, P.; Mendricky, R.; Safka, J. Parameters influencing the precision of various 3d printing technologies. *MM Sci. J.* **2017**, *5*, 2004–2012. [CrossRef]
29. *ISO 17295:2023*; Additive Manufacturing—General Principles—Part Positioning, Coordinates and Orientation. ISO: Geneva, Switzerland, 2023.
30. Dizon, J.R.C.; Gache, C.C.L.; Cascolan, H.M.S.; Cancino, L.T.; Advincula, R.C. Post-processing of 3D-printed polymers. *Technologies* **2021**, *9*, 61. [CrossRef]
31. Tamburrino, F.; Barone, S.; Paoli, A.; Razionale, A.V. Post-processing treatments to enhance additively manufactured polymeric parts: A review. *Virtual Phys. Prototyp.* **2021**, *16*, 221–254. [CrossRef]
32. *ISO 8015:2011*; Geometrical Product Specifications (GPS)—Fundamentals—Concepts, Principles and Rules. ISO: Geneva, Switzerland, 2011.
33. *ISO 1101:2017*; Geometrical Product Specifications (GPS)—Geometrical Tolerancing—Tolerances of Form, Orientation, Location and Run-Out. ISO: Geneva, Switzerland, 2017.
34. *ISO 286-2:2010*; Geometrical Product Specifications (GPS)—ISO Code System for Tolerances on Linear Sizes—Part 2: Tables of Standard Tolerance Classes and Limit Deviations for Holes and Shafts. ISO: Geneva, Switzerland, 2010.
35. *ISO 22081:2021*; Geometrical Product Specifications (GPS)—Geometrical Tolerancing—General Geometrical Specifications and General Size Specifications. ISO: Geneva, Switzerland, 2021.
36. *ASME Y14.5*; Dimensioning and Tolerancing. ASME: New York, NY, USA, 2018.
37. *ISO 21920-1:2021*; Geometrical Product Specifications (GPS)—Surface Texture: Profile—Part 1: Indication of Surface Texture. ISO: Geneva, Switzerland, 2021.
38. *ISO 21920-2:2021*; Geometrical Product Specifications (GPS)—Surface Texture: Profile—Part 2: Terms, Definitions and Surface texture parameters. ISO: Geneva, Switzerland, 2021.
39. *ISO 21920-3:2021*; Geometrical Product Specifications (GPS)—Surface Texture: Profile—Part 3: Specification Operators. ISO: Geneva, Switzerland, 2021.
40. Yadav, D.K.; Srivastava, R.; Dev, S. Design & fabrication of ABS part by FDM for automobile application. *Mater. Today Proc.* **2020**, *26*, 2089–2093. [CrossRef]
41. Ilyas, R.A.; Sapuan, S.M.; Harussani, M.M.; Hakimi, M.Y.A.Y.; Haziq, M.Z.M.; Atikah, M.S.N.; Asrofi, M. Polylactic acid (PLA) biocomposite: Processing, additive manufacturing and advanced applications. *Polymers* **2021**, *13*, 1326. [CrossRef]
42. Spoerk, M.; Holzer, C.; Gonzalez-Gutierrez, J. Material extrusion-based additive manufacturing of polypropylene: A review on how to improve dimensional inaccuracy and warpage. *J. Appl. Polym. Sci.* **2020**, *137*, 48545. [CrossRef]
43. Singh, S.; Ramakrishna, S.; Singh, R. Material issues in additive manufacturing: A review. *J. Manuf. Process* **2017**, *25*, 185–200. [CrossRef]
44. Trivedi, A.K.; Gupta, M.; Singh, H. PLA based biocomposites for sustainable products: A review. *Adv. Ind. Eng. Polym. Res.* **2023**, *6*, 382–395. [CrossRef]
45. Figueroa-Cavazos, J.O.; Flores-Villalba, E.; Diaz-Elizondo, J.A.; Martínez-Romero, O.; Rodríguez, C.A.; Siller, H.R. Design Concepts of Polycarbonate-Based Intervertebral Lumbar Cages: Finite Element Analysis and Compression Testing. *Appl. Bionics Biomech.* **2016**, *2016*, 7149182. [CrossRef] [PubMed]
46. Additive Manufacturing Reduces Tooling Cost and Lead Time to Produce Composite Aerospace Parts Parent Categ. 3D Print. News (/en/3d), Categ. Aerosp. Publ. Available online: http://globalprintmonitor.de/en/3d/3d-printing-new (accessed on 28 October 2024).
47. Achillas, C.; Tzetzis, D.; Raimondo, M.O. Alternative Production Strategies Based on the Comparison of Additive and Traditional Manufacturing Technologies. *Int. J. Prod. Res.* **2017**, *55*, 3497–3509. [CrossRef]
48. Hanssen, J. *Fortus 360 mc/400 mc Accuracy Study*; Stratasys White Paper; Stratasys, Ltd.: Rehovot, Israel, 2017.
49. Cekic, A.; Muhamedagic, K.; Begic-Hajdarevic, D.; Djuzo, N. Effect of Process Parameters on Dimensional Accuracy and Tensile Strength of FDM Printed Parts. In Proceedings of the 31st DAAAM International Symposium, Mostar, Bosnia and Herzegovina, 21–24 October 2020; pp. 66–71. [CrossRef]

50. Favier, V.; Zemiti, N.; Caravaca Mora, O.; Subsol, G.; Captier, G.; Lebrun, R.; Gilles, B. Geometric and mechanical evaluation of 3D-printing materials for skull base anatomical education and endoscopic surgery simulation–A first step to create reliable customized simulators. *PLoS ONE* **2017**, *12*, e0189486. [CrossRef] [PubMed]
51. Ai, J.R.; Peng, F.; Joo, P.; Vogt, B.D. Enhanced dimensional accuracy of material extrusion 3D-printed plastics through filament architecture. *ACS Appl. Polym. Mater.* **2021**, *3*, 2518–2528. [CrossRef]
52. Aldawood, F.K.; Chang, S.X.; Desai, S. Design and manufacture of a high precision personalized electron bolus device for radiation therapy. *Med. Devices Sens.* **2020**, *3*, e10077. [CrossRef]
53. Vidakis, N.; Petousis, M.; David, C.; Sagris, D.; Mountakis, N.; Moutsopoulou, A. Polycarbonate hybrid friction stir welding joints: Welding forces and quality indicators on 3D printed and solid sheets single and two-axis seams. *Int. J. Adv. Manuf. Technol.* **2024**, *134*, 431–444. [CrossRef]
54. Reyes-Rodríguez, A.; Dorado-Vicente, R.; Mayor-Vicario, R. Dimensional and form errors of PC parts printed via Fused Deposition Modelling. *Procedia Manuf.* **2017**, *13*, 880–887. [CrossRef]
55. Mendricky, R.; Fris, D. Analysis of the accuracy and the surface roughness of fdm/fff technology and optimisation of process parameters. *Teh. Vjesn.* **2020**, *27*, 1166–1173. [CrossRef]
56. Jiang, S.; Hu, K.; Zhan, Y.; Zhao, C.; Li, X. Theoretical and experimental investigation on the 3D surface roughness of material extrusion additive manufacturing products. *Polymers* **2022**, *14*, 293. [CrossRef]
57. García, E.; Núñez, P.J.; Chacón, J.M.; Caminero, M.A.; Kamarthi, S. Comparative study of geometric properties of unreinforced PLA and PLA-Graphene composite materials applied to additive manufacturing using FFF technology. *Polym. Test.* **2020**, *91*, 106860. [CrossRef]
58. García Plaza, E.; López, P.J.N.; Torija, M.Á.C.; Muñoz, J.M.C. Analysis of PLA geometric properties processed by FFF additive manufacturing: Effects of process parameters and plate-extruder precision motion. *Polymers* **2019**, *11*, 1581. [CrossRef] [PubMed]
59. Alsoufi, M.S.; Elsayed, A.E. How surface roughness performance of printed parts manufactured by desktop FDM 3D printer with PLA+ is influenced by measuring direction. *Am. J. Mech. Eng.* **2017**, *5*, 211–222. [CrossRef]
60. Buj-Corral, I.; Domínguez-Fernández, A.; Durán-Llucià, R. Influence of print orientation on surface roughness in fused deposition modeling (FDM) processes. *Materials* **2019**, *12*, 3834. [CrossRef] [PubMed]
61. Milde, J.; Jurina, F.; Peterka, J.; Dobrovszký, P.; Hrbál, J.; Martinovič, J. Influence of part orientation on the surface roughness in the process of Fused Deposition Modeling. *Key Eng. Mater.* **2021**, *896*, 29–37. [CrossRef]
62. Pawar, S.; Dolas, D. Effect of process parameters on flexural strength and surface roughness in fused deposition modeling of PC-ABS material. *J. Micromanuf.* **2022**, *5*, 164–170. [CrossRef]
63. Naat, N.; Boutar, Y.; Mezlini, S.; da Silva, L.F.; Alrasheedi, N.H.; Hajlaoui, K. Study of the effect of bio-inspired surface texture on the shear strength of bonded 3D-printed materials: Comparison between stainless steel and polycarbonate joints. *Int. J. Adhes. Adhes.* **2024**, *131*, 103658. [CrossRef]
64. Bazan, A.; Turek, P.; Przeszłowski, Ł. Comparison of the contact and focus variation measurement methods in the process of surface topography evaluation of additively manufactured models with different geometry complexity. *Surf. Topogr. Metrol. Prop.* **2022**, *10*, 035021. [CrossRef]


**Disclaimer/Publisher's Note:** The statements, opinions and data contained in all publications are solely those of the individual author(s) and contributor(s) and not of MDPI and/or the editor(s). MDPI and/or the editor(s) disclaim responsibility for any injury to people or property resulting from any ideas, methods, instructions or products referred to in the content.